

NJC

Accepted Manuscript



This is an *Accepted Manuscript*, which has been through the Royal Society of Chemistry peer review process and has been accepted for publication.

Accepted Manuscripts are published online shortly after acceptance, before technical editing, formatting and proof reading. Using this free service, authors can make their results available to the community, in citable form, before we publish the edited article. We will replace this *Accepted Manuscript* with the edited and formatted *Advance Article* as soon as it is available.

You can find more information about *Accepted Manuscripts* in the [Information for Authors](#).

Please note that technical editing may introduce minor changes to the text and/or graphics, which may alter content. The journal's standard [Terms & Conditions](#) and the [Ethical guidelines](#) still apply. In no event shall the Royal Society of Chemistry be held responsible for any errors or omissions in this *Accepted Manuscript* or any consequences arising from the use of any information it contains.



www.rsc.org/njc

Ga doped RGO-TiO₂ composite on ITO surface electrode for investigation of photoelectrocatalytic activity under visible light irradiation

Md. Rakibul Hasan^{1, a}, Sharifah Bee Binti Abdul Hamid^{1, b}, Wan Jeffrey Basirun^{1, c},
Zaira Zaman Chowdhury^{1, d}, Ahmad Esmailzadeh Kandjani^{2, e}, Suresh K Bhargava^{2, f}.

¹Nanotechnology & Catalysis Research Center (NANOCAT), 3rd floor, Block A, Institute of Postgraduate Studies (IPS), University of Malaya, 50603 Kuala Lumpur, Malaysia.

²Centre of Advanced Materials & Industrial Chemistry, School of Applied Science, RMIT University, GPO BOX 2476, Melbourne 3000, Australia

^arakibacctu@gmail.com, ^bsharifahbee@um.edu.my, ^cwjeffreyb@yahoo.com, ^dzaira.chowdhury76@gmail.com,
^eahmad.kandjani@rmit.edu.au, ^fsuresh.bhargava@rmit.edu.au

ABSTRACT:

Gallium (Ga) doped reduced graphene oxide-titania (RGO-TiO₂) composites were successfully synthesized by sol-gel method and deposited on ITO coated glass substrate via electrophoretic deposition method. The photocatalyst materials were tested for CO₂ conversion reaction in aqueous media. Prior to this, the catalysts were characterized by X-ray diffraction (XRD), scanning electron microscopy (SEM), UV-vis reflectance spectroscopy and Fourier transformed infrared spectroscopy (FTIR). The synergistic effect of RGO and Ga doping on TiO₂ was investigated. Electron/hole recombination on the catalyst surface can be minimized greatly by using RGO with TiO₂ while Ga doping assists to reduce the band gap energy. The corresponding expansion of the absorption range towards the visible region was also observed. The results showed that, both RGO and Ga enhance the CO₂ adsorption on the catalyst surface, hence facilitates high CO₂ conversion yield. The photoreduction products were mostly formic acid and trace amount of methanol. Higher yield of formic acid was shown by the Ga-RGO-TiO₂ composite films compared to the RGO-TiO₂ composite and pure TiO₂ film during a 120 min period of visible light irradiation.

KEYWORDS: RGO, nanocomposites, CO₂ reduction, photoelectrocatalysis, solar simulator

1.0 INTRODUCTION

Present day life of human being is very much influenced by energy and environment related problems as the world total energy consumption is still dependent on conventional energy resources rather than renewable energy [1]. Burning of fossil fuels (natural gas, coal, petroleum etc.) releases carbon dioxide (CO₂) in the atmosphere. The environment is increasingly affected by the so called greenhouse effect with the increase of CO₂ concentration in the atmosphere [2]. Hence, mitigation of CO₂ in the atmosphere with the help of abundant renewable energy sources is becoming one of the key areas of present day research. CO₂ conversion process is not a new phenomenon and processes such as chemical reduction, thermochemical, photochemical, electrochemical conversions are already been established [3]. Although some conversion processes have been practiced in an industrial scale [4], the conversion yield is unsatisfactory and hence are not economically feasible. Although the catalytic reduction of CO₂ to hydrocarbons (i.e. formic acid, methanol, methane etc.) using hydrogen gas as a reducing agent is attainable, a renewable energy source which closely mimics the photosynthetic process to produce synthetic fuels should be involved in the total conversion process to attain feasibility. Hence the photoreduction of CO₂ in aqueous media draws attention in this context [5].

Solar energy is a viable renewable energy source due to its abundance and availability [6]. The photoreduction of CO₂ using solar energy is a process which can readily couple this free energy with inexpensive reducing agent (i.e. water) to achieve rapid and selective production of various hydrocarbon fuels such as HCHO, CH₃OH, HCOOH, CH₄ etc [7]. Furthermore, some of the reduced species could be a valuable feedstock as industrial raw materials for various processes.

The key role in the total conversion process depends on an efficient photocatalytic material for solar irradiation. Various metal oxides and carbon nanomaterials such as WO_3 , TiO_2 , CdS , GaP , ZrO_2 , ZnO , SiC , graphene, and carbon nanotubes (CNTs) have been studied [8,9]. Among them, the wide band gap TiO_2 photocatalyst (3.2 eV) is considered the most appropriate metal oxides due to their promising features. Titania nanomaterials are commercially established photocatalytic material. The reasons are due to its wonderful tunable microstructure, chemical stability, non-toxicity, easy availability and low cost [10]. Graphene, a two dimensional layer of sp^2 hybridized carbon atoms in honeycomb structure has attracted great interest in the development of advanced nanomaterials [11] due to its excellent optical, thermal, electrical and mechanical properties. Graphene has seen applications in the fabrication of catalyst, capacitors and biosensors due to these exceptional features. Due to the absence of functional groups and low solubility of graphene in most common solvents, the more soluble graphene oxide and reduced graphene oxide have been used in these applications [12].

Graphene oxide (GO) in its reduced form i.e. reduced graphene oxide (RGO) has less defect sites, hence shows high electron mobility and optical transparency [13]. Large specific surface area, strong mechanical properties and high stability are the unique properties of RGO as electrocatalyst and photocatalyst materials [14]. In the field of photocatalysis, both TiO_2 and RGO are very attractive material due to their light absorption properties and stability [15]. Recent research showed that, RGO- TiO_2 composite can be used for photodegradation of pollutants, solar cells and H_2 production [16]. Some reports on CO_2 conversion using RGO- TiO_2 composite are also available [5].

Utilization of solar energy in the visible region which forms almost 40% of the total solar spectrum can be achieved by using semiconductor with an appropriate band gap. TiO_2 nanomaterials still have some limitations to be photocatalytically activated under the visible region. Fast photogenerated charge recombination rate is still a major drawback to achieve higher photocatalytic efficiency [17].

The photoelectrocatalysis (PEC) process, which combines photocatalysis and electrochemical redox process, can minimize the charge recombination losses and photo-instabilities of the photo-excited semiconductors [18] to a great extent. In this case, the immobilization of photocatalyst powder onto a conducting substrate is an efficient strategy for successful PEC process [19]. Hence, there is still plenty of opportunity to enhance the photocatalytic efficiency of TiO_2 nanomaterials.

For this reason, higher efficiency could be reached by replacing Ti ($3d^0$) atoms with $3d^{10}$ Ga cations thus inducing O 2p vs cation $3d^{10}$ repulsion. The coupling of TiO_2 with Ga_2O_3 can promote easy electron-hole separation process under irradiation and decreasing the recombination effect for higher photocatalytic activity. Furthermore Ga_2O_3 are also effective activation site for the reaction of CO_2 molecule [20].

In this work, Ga-RGO- TiO_2 nanocomposite powder produced by acid catalyzed sol-gel process was deposited onto ITO substrate via electrophoretic deposition. The thin film catalyst was assembled in a PEC reactor for the photo-catalytic reduction of CO_2 under solar simulator irradiation.

2.0 EXPERIMENTAL METHODS

2.1 Materials

Graphite flake nominally sized at 7-10 μm was procured from Alfa Aesar. Tetra-n-butyl ortho titanate [$\text{Ti}(\text{OBu})_4$] was procured from Sigma-Aldrich and all other chemicals used in this work were of analytical grade. The indium tin oxide (ITO) coated conducting glass plates (0.7 mm thickness) were procured from Osaka, Japan. Deionized water (18.2 M Ω cm) used for all experiments was obtained from a Milli-Q system (Millipore, Bedford. with Mega-Pure System, Model MP-290). The light source, 150 W (Xe arc lamp) solar simulator was purchased from OSRAM photo optic, Germany. It has a consistent spectrum profile of sunlight i.e. almost same characteristic features of solar light under standard air condition. Carbon dioxide was used from gas cylinder containing 99.9% pure gas.

2.2 Preparation of reduced graphene oxide (RGO)

Graphene oxide (GO) was prepared with the modified Hummer's method [21-23]. 1 g graphite flakes was mixed with sulfuric acid and phosphoric acid (120 ml:13 ml). Then 6 g KMnO_4 was gradually added and the mixture was kept under stirring for 3 days. Then with the addition of 7 ml H_2O_2 solution (30%) and 135 ml ice water, the mixture turned brown color. The mixture was then centrifuged at 4000 rpm for 10 minutes. After the centrifugation process the GO suspension was washed with 1M HCl via the same sonication process. The GO suspension was dried in an oven and later subjected to hydrazine treatment to obtain reduced graphene oxide (RGO) [24]. 300 mg of GO powder was mixed with 600 ml ultrapure milli-Q water and kept under sonication for 15 minutes. Then 3ml hydrazine hydrate was added and the solution was kept under vigorous stirring at 90°C for 6 hours. The RGO was precipitated as a black solid [25]. The solution was filtered and washed with ethanol and water several times to obtain the RGO powder. The powder was dried in an oven at 80°C .

2.3 Preparation of Ga-RGO- TiO_2 nanocomposite

For the preparation of TiO_2 nanocomposite, 20 ml TBOT was added with 80ml of absolute ethanol and kept under stirring. Then 6 ml ultrapure water, 6 ml ethanol, 1mol% $\text{Ga}(\text{NO}_3)_3 \cdot x\text{H}_2\text{O}$ and 1wt% RGO powder was mixed and kept under sonication for 1.5 hours. This mixture was added with the TBOT solution dropwise for 30 minutes. Acetic acid was added to lower the pH of the solution to < 3 . The total mixture was kept under vigorous stirring for 30 minutes to obtain a homogeneous solution. The dark colored solution was then kept at room temperature for 48 hours for proper gel formation. The gel was dried at 100°C overnight. The dry porous gel was milled with a steel made mortar and pestle. The fine powder catalyst was then calcined at 550°C for 4 hours.

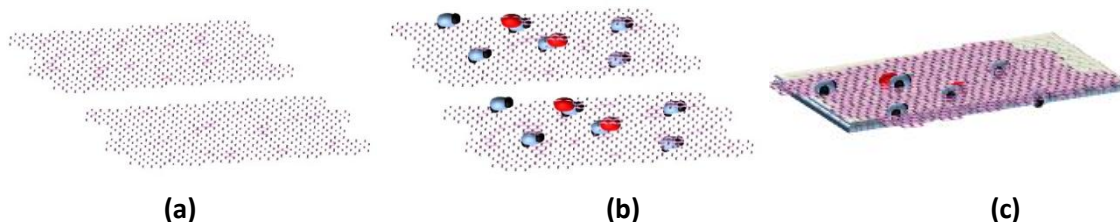


Figure 1: Schematic diagram of the (a) RGO (b) Ga-RGO- TiO_2 composite (c) Ga-RGO- TiO_2 /ITO thin film.

2.4 Fabrication of Ga-RGO- TiO_2 /ITO photoanodes

The Ga-RGO- TiO_2 /ITO films were synthesized using electrophoretic deposition method. The prepared composite powder was dispersed in DI water at a concentration of 0.1 mg ml^{-1} , at pH ~ 3.5 . The mixture was sonicated to ensure a homogeneous dispersion of the composite powder before the deposition process. Figure 1 shows the preparation steps where 1(c) shows the Ga-RGO- TiO_2 /ITO photocatalyst thin film.

2.5 Photoelectrochemical measurements

All photoelectrochemical measurements were done in a cubic quartz cell using an Autolab PGSTAT30 potentiostat/galvanostat (Ecochemie, Netherlands). A standard three-electrode system was used where the photoanodes with an area of 1 cm^2 were the working electrode (WE). A platinum (Pt) wire was the counter electrode and a saturated calomel electrode (SCE) was the reference. The electrolyte used in these experiments was $0.1 \text{ M Na}_2\text{SO}_4$. The voltammetric measurement was done in a potential range of 0.0 V to -1.5 V (vs SCE) with a scan rate of 50 mV s^{-1} . Electrochemical impedance spectroscopy (EIS) was measured at the open circuit potential (OCP) in the dark and under solar simulator irradiation. Simulation of the EIS experimental data was done using analog circuits with the NOVA 1.9 software installed in a computer, interfaced with the potentiostat. The frequency range was between 10^{-1} Hz to 10^5 Hz , with amplitude of 5 mV around the OCP.

2.6 Constant potential photoelectrolysis

The photoelectrocatalytic conversion of CO₂ was conducted in the quartz cell containing 5% triethanolamine (TEA) aqueous solution. Figure 2 shows a schematic diagram of the photoelectrocatalytic reduction process with a three-electrode system, where a Pt wire was the CE with the area as the WE. The irradiation intensity was measured as ~10 mW cm⁻². Prior to the reaction, CO₂ was bubbled for 1 hour to produce a saturated solution. The liquid phase product was analyzed by gas chromatography-mass spectroscopy. Formic acid concentration was measured by a gas chromatography (Agilent 6890N with 5973 mass selective detector). The temperature profile for the detection method was: injector 250°C, oven 40°C and the detector at 180°C. Only the peaks for formic acid and methanol were taken into account during the chromatography process.

2.7 Apparatus and measurements

A scanning electron microscope (SEM, Quanta FEI 200) was used to assess the morphology of as-prepared composite samples. The X-ray diffraction (XRD) measurements were recorded with a powder X-ray diffractometer (Type Bruker D8 Advance equipped with EVA diffract software, Germany) over the range 20° ≤ 2θ ≤ 80°, operating at 40kV and 30 mA with a Cu Kα radiation (λ = 1.5418 Å). UV-Vis absorbance spectra were obtained by a spectrophotometer from Perkin Elmer, Lambda 35 series equipped with a 10 mm path length quartz cell. Fourier transformed infrared spectroscopy (FTIR) was recorded using a Bruker IFS 66V/S using a KBr technique.

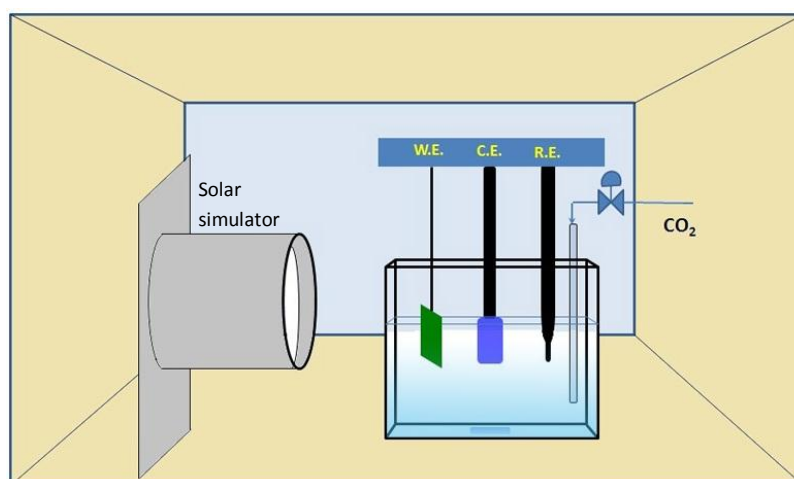


Figure 2: Quartz made photoelectrocatalytic (PEC) reactor with solar simulator.

X-ray photoelectron spectroscopy (XPS) surface analyses were carried out using a flat gold (Si/10nm Ti/200nm Au) as the substrate and reference. Thermo Scientific K-alpha instrument with an unmonochromatized Mg Kα radiation (photon energy 1253.6 eV) source and vacuum better than 10⁻⁹ Torr as well as spectral resolution of 0.1 eV was used for XPS studies. XPS core levels were aligned to the Au 4f 7/2 binding energy (BE) of 84 eV.

3.0 RESULTS AND DISCUSSION

3.1 Fabrication and Characterization of the Ga-RGO-TiO₂/ITO composite electrode

The catalyst film was characterized in crystallographic, morphological and optical analyses. XRD revealed the crystalline phases of TiO₂ anatase. Figure 3 shows the XRD pattern of the prepared catalyst. According to the JCPDS ref. code 01-086-1157, the characteristic sharp peaks at 25.3 (101), 37.9 (103), 48.1 (200), 53.9 (105), 75.1(215) confirms titania tetragonal crystal system of anatase phase. The calcination temperature 550 °C mainly played the role to produce crystalline nanocomposites of TiO₂ anatase. No phase change of anatase to rutile was found. 37.6 and 38.5 peaks could be of β-Ga₂O₃ phase as well along with TiO₂ phase [JCPDS ref. code 00-011-0370]. Other peaks at 30.5, 31.7, 33.5, 35.2, 42.9, 46.2, 48.6° for characteristic Ga₂O₃ were not observed in the prepared sample. This is due to Ga₂O₃ doping concentration was too low and it was beyond X-ray diffraction limit. the peak overlapping of RGO characteristic peak at 25.8° with TiO₂ (101) plane was observed. It can be assumed that, Ga₂O₃ was highly dispersed on TiO₂

surface and hence the peaks corresponding Ga_2O_3 are not obvious. The average crystallite size was calculated using Scherrer's formula (eq. 1) in respect of anatase (101) peak.

$$D = \frac{\kappa\lambda}{\beta\cos\theta}, \quad (1)$$

Where, D = crystallite size, λ = wavelength of X-ray, β = full width at half maximum of the peak (in radians) and θ = angle of diffraction (in degrees).

The crystallite size for the Ga-RGO- TiO_2 composites was between 35~56 nm. Doping of RGO didn't bring any crystallite phase changes. Thus it can be said that, RGO has no effect on crystallite size.

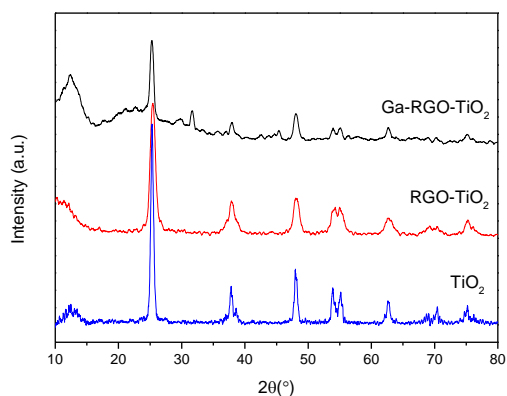


Figure 3: XRD pattern of TiO_2 , RGO- TiO_2 and Ga-RGO- TiO_2

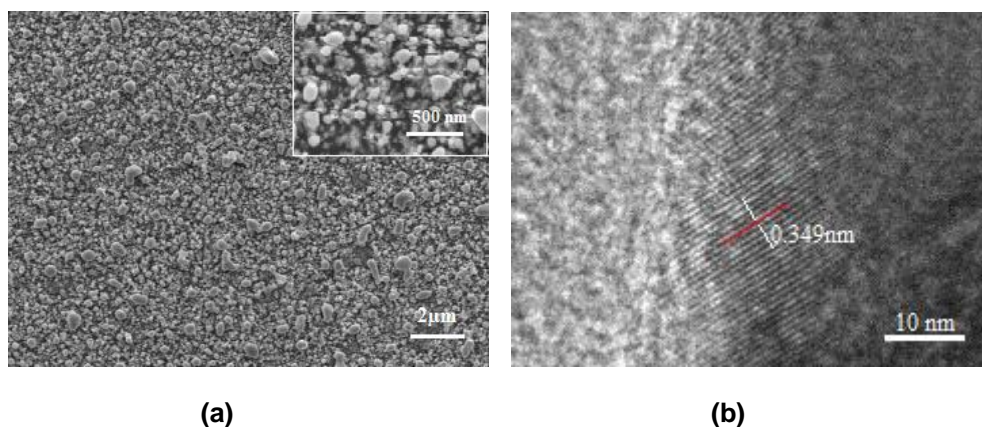


Figure 4: SEM image (a) and TEM image (b) of Ga-RGO- TiO_2

Figure 4 (a) shows the FESEM image of Ga-RGO- TiO_2 composite nanoparticles. It was observed that, the sample particles were quite irregular spheres whereas pure TiO_2 were mostly spherical (not shown here). Thus the influence of the dopants on the morphology of catalyst is obvious. The morphological change may be due to the formation of grain boundaries at high temperature calcination. On the other hand, the d-spacing for Ga-RGO- TiO_2 composite were estimated from HRTEM to be 0.349 nm Figure 4(b). The relative higher value for Ga doped RGO- TiO_2 composite ensures successful doping of other elements into TiO_2 lattice. The particle size was found to be about 120-160 nm in diameter. It can be assume that Ga-RGO- TiO_2 particles are aggregates of small crystals.

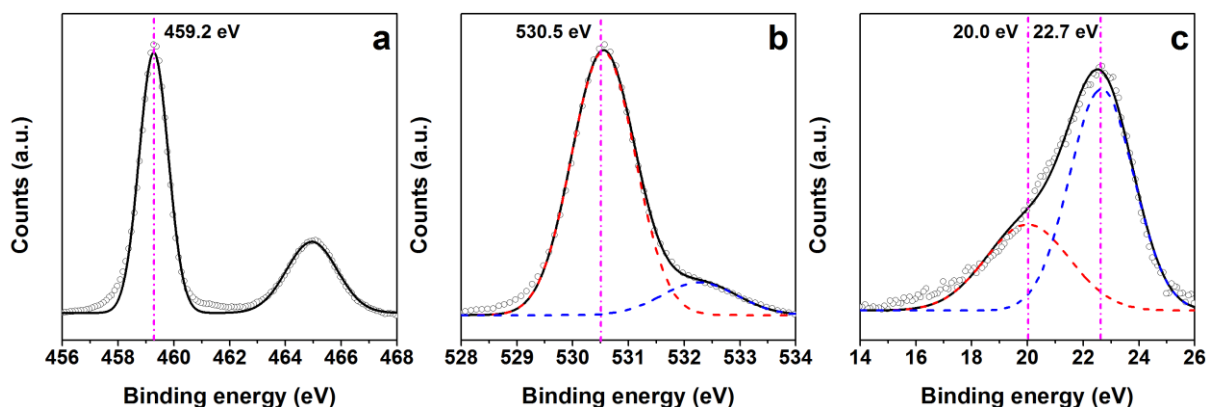


Figure 5. XPS spectra of a) Ti 2p, b) O 1s and c) Ga 3d for Ga doped TiO₂ nanoparticles

Figure 5 shows XPS spectra of Ga doped TiO₂ nanoparticles. The electron-binding energy (BE) of the photoelectron peak of Ti 2p (Fig. 5a) illustrates the existence of Ti⁴⁺ species in TiO₂ nanostructures located at 459.2 eV. The shift could be related to the electron interaction between doped Ga and Ti in the structure. It has been previously [26] shown that the doping of semiconductors with Ga can make a significant shift on Ga³⁺ 3d peak to higher energies. Similarly in this work, the two peaks observed in the Ga doped spectrum (Fig. 5c) shifting towards higher energies can be contributed to the formation of free Ga³⁺ and Ga²⁺ (20.0 and 22.7 eV) in the structures, respectively [27,28]

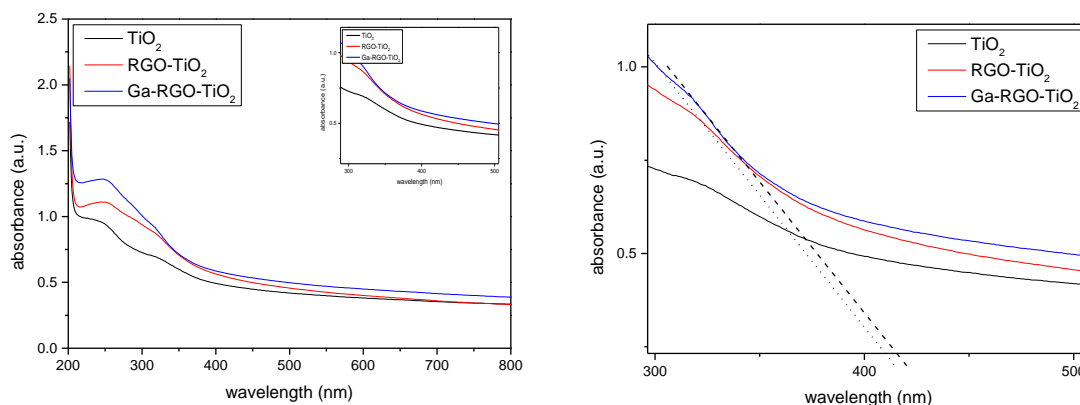


Figure 6: UV-Vis spectra of Ga-RGO-TiO₂ nanocomposite and broader peak (inset and left).

Figure 6 depicts the UV-Vis absorbance spectra to Ga-RGO-TiO₂ nanoparticles in the range of 200-800nm. The curve reflects the optical absorption property of the catalyst. The sample clearly exhibits red shift of absorption edge toward the visible region. The peak was found a bit splitted and a part of it shows absorption in the visible region which is more than pure TiO₂ (absorption <387 nm) and the absorption range is wider than pure TiO₂ and Gr-TiO₂ as well. The band gap values were determined by the equation (2),

$$E_{bg} = \frac{1240}{\lambda} \text{ (eV)} \quad (2)$$

Where, E_{bg} = band gap energy of the photocatalyst material and λ = maximum wavelength in nm
The band gap value obtained by calculation ranges from 2.95 to 3.35 eV.

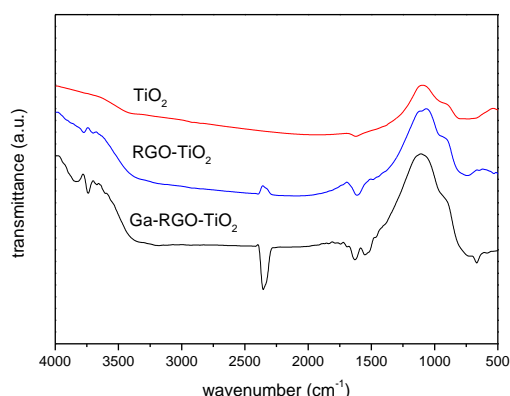


Figure 7: FTIR spectra of TiO_2 , RGO-TiO_2 and Ga-RGO-TiO_2

The FTIR spectrum of the prepared catalyst sample is shown in Figure 7. The prominent absorption bands were observed at 468.16 , 666 , 1551 , 1626 cm^{-1} . In RGO, most of the C=O bond are eliminated therefore the peak at 1720cm^{-1} was absent. It confirms well reduced RGO structure. The peak at 1551 cm^{-1} is attributed to graphene sheet skeletal vibration. Ti-O-Ti stretching vibrational peak was observed below 1000cm^{-1} . The broader peak in the range $2400\text{-}3400\text{cm}^{-1}$ can be attributed to H-bonding between -OH groups present on TiO_2 surface. Ga-O stretching vibration absorption was observed at 468.16cm^{-1} and it denotes to monoclinic Ga_2O_3 structure [29]. A strong peak at 2358cm^{-1} is due to adsorbed CO_2 molecule on the TiO_2 surface for atmospheric CO_2 .

The most critical drawback in photoelectrocatalysis is the recombination process [30]. EIS is a quite useful tool to investigate the charge transfer and recombination processes at the semiconductor/electrolyte interface [31]. The EIS responses of $\text{Ga-RGO-TiO}_2/\text{ITO}$ are shown as Nyquist plots corresponding to the imaginary part Z'' versus the real part Z' of the complex impedance Z (Figure 8). The impedance values of the photocatalyst were measured at open circuit potential in dark and illumination conditions. While under irradiation, the diameter of loop decreases and the curve tends to become a semicircle. The charge transfer resistance (R_{ct}) is the manifestation of the electron transfer kinetics across the electrode/electrolyte interface [32]. A straight slope at lower frequencies is due to the diffusion process between the electrode and the electrolyte. Figure 7 inset, shows the equivalent circuit across the electrode/electrolyte interface where a Warburg diffusion model is proposed. Here, R_e refers to the bulk resistance between the WE and the RE, at the high frequency intercept of the semicircle with respect to the real axis. The interfacial resistance is described by R_{CT} in the circuit. The low frequency region where almost a straight line was observed is represented by the Warburg impedance (W). This impedance apparently results from the OH^- or H^+ ion diffusion on the electrode surface [33].

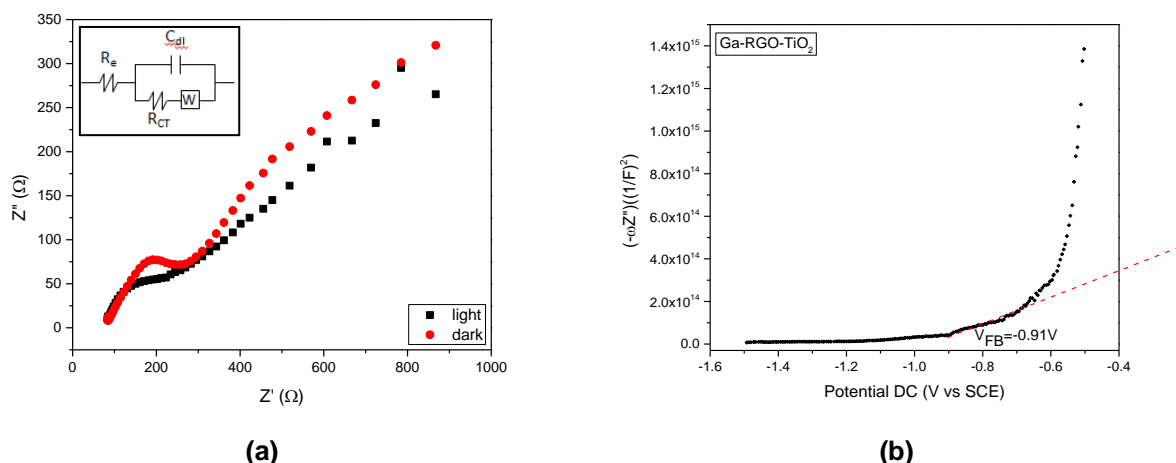


Figure 8: The EIS impedance spectra (Nyquist plots) of the Ga-RGO-TiO₂ film electrodes (fig. 7a) with (black) and without (red) light irradiation at open circuit potential. Mott-Schottky analysis of Ga-RGO-TiO₂ photoelectrode at DC potential range of -1.5 to -0.5V_{SCE} at pH 6.8 (fig. 7b)

A positive slope in the Mott-Schottky plot in Fig. 7b indicates that the photocatalyst is n-type.

3.2 Photoelectrocatalytic reduction of carbon dioxide into formic acid

Figure 9 shows the voltammetric response of the catalyst film under different conditions. In the dark, no current was observed (Fig. 9 a). A small current was observed when the catalyst thin film was illuminated (Fig. 9b). After 1 hour CO₂ bubbling, the pH of the 5% triethanolamine (TEA) solution was 6.8.

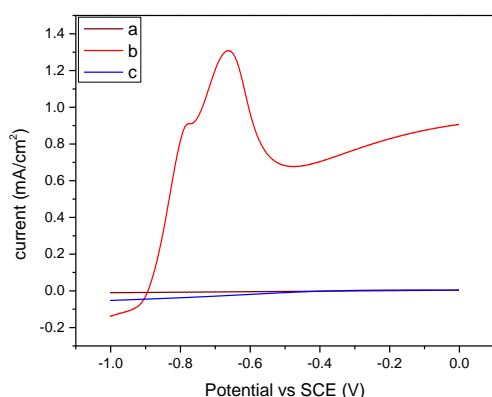
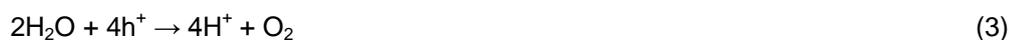


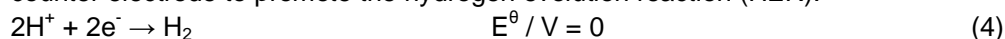
Figure 9: Voltammetric response of the illuminated Ga-RGO-TiO₂/ITO electrode in presence of 5%TEA solution (a) in the dark, (b) under illumination with solar simulator and (c) under illumination with CO₂.

A significant anodic current can be seen in the presence of CO₂ (Fig. 8c). The anodic peak at about -0.57 V (vs SCE) is due to the presence of CO₂ in the TEA solution. In addition, the peak current increased with the concentration of TEA solution.

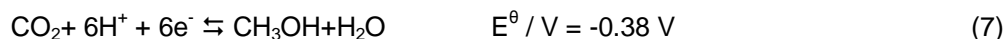
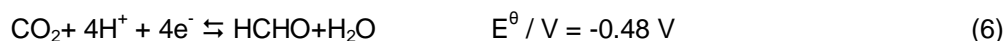
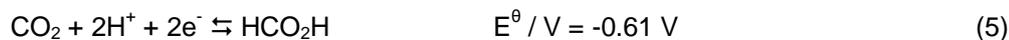
When the catalyst was illuminated, electrons from the valence bands are excited to the conduction bands and leaving holes where water oxidation occurs as follows:



The excited electrons complete the circuit and reach the counter electrode. The electrons which reach the counter electrode to promote the hydrogen evolution reaction (HER):



When in the presence of CO_2 , it was observed that gas bubbles evolved on the platinum counter electrode. Apart from this, CO_2 reduction also commenced with the release of electrons from the photoanode. With the reactions at the platinum counter electrode purely electrochemical, comparisons of the standard equilibrium potentials for the reduction of CO_2 with the HER can be given as [34]:



The low concentration of formic acid observed is due to the CO_2 reduction harder to achieve compared to the HER.

Constant potential photoelectrolysis experiment was done at -0.57 V vs SCE and resulted in low Faradaic efficiency of formic acid. Figure 9(a) shows that the concentration of formic acid increases with the electrolysis time (max. 178 ppm in 2 hours). The presence of formic acid is detected as the reduction product by both HPLC and GC-MS. Figure 9(b) presents the graph of photocurrent vs reaction time. A constant photocurrent of 1.5 mA cm^{-2} persisted for almost 40 minutes. The initial drop of photocurrent was observed from 4.6 mA to 1.65 mA during the first 30 minutes. A schematic mechanism of CO_2 photoconversion into HCOOH is shown in Figure 10.

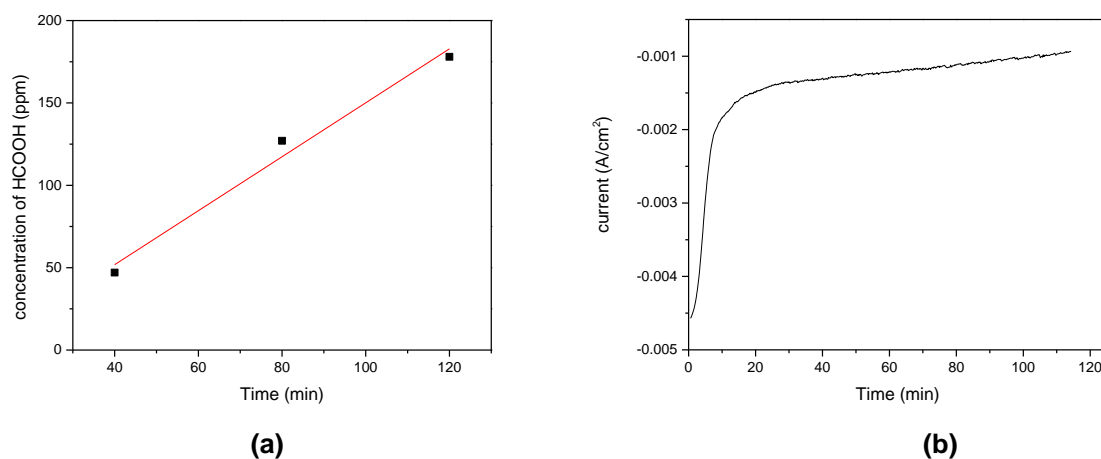


Figure 9 : Yield of formic acid as a function of reaction time (a) and dependence of photocurrent on reaction time in photoelectrocatalytic reduction of CO_2 (b)

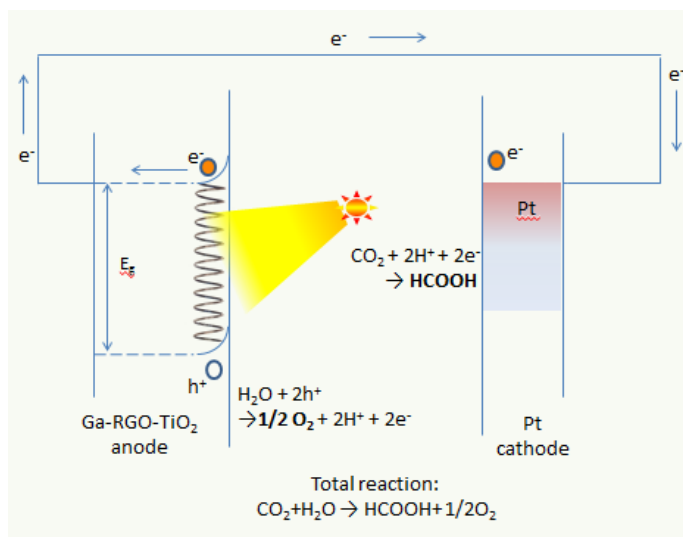


Figure 10: Schematic of the photoelectrocatalysis of CO₂

4.0 CONCLUSIONS:

Ga doped RGO-TiO₂ composite was fabricated via a sol-gel process and deposited on ITO substrate with electrophoretic deposition method. The XRD diffractograms show that the samples are well crystallized which is a key factor for successful photocatalytic activity. The nanostructured surface morphology with Ga doped sample enhances photoconversion process of CO₂ to a great extent. Ga doping also helps the RGO-TiO₂ nanomaterial to absorb light irradiation in visible region (>400nm wavelength). The photocurrent was raised at maximum 4.6mA at -0.57V bias potential on Ga-RGO-TiO₂/ITO photoelectrode. No significant photocurrent was observed for TiO₂ or RGO-TiO₂ thin film photoelectrodes. Maximum 178 ppm of formic acid was recorded for two hours reaction period. The low concentration of formic acid produced at the counter electrode is due to the vigorous HER at the platinum surface. Nevertheless the concentration of the formic acid increased with the photoelectrolysis reaction time.

Acknowledgements

The authors would like to thank University of Malaya for sponsoring this work under National Nanotechnology Directorate (NND-53-02031090), High Impact Research (HIR-F-000032) and IPPP grant (PG043-2012B) for their cordial support to complete this work.

REFERENCES

- [1] Demirbas, A. (2005), Progress in Energy and Combustion Science **31**(2): 171-192.
- [2] Solomon, S., G. K. Plattner, R. Knutti and P. Friedlingstein (2009), Proc Natl Acad Sci U S A **106**(6): 1704-1709.
- [3] Scibioh, M. A. and B. Viswanathan (2004), Proc Indian Natn Sci Acad **70 A**(3): 407-462.
- [4] Madikizela, N. N. and N. J. Coville (2002), Journal of Molecular Catalysis A: Chemical(181): 129-136.
- [5] Handoko, A. D., K. Li and J. Tang (2013), Current Opinion in Chemical Engineering **2**(2): 200-206.
- [6] Roy, S. C., O. K. Varghese, M. Paulose and C. A. Grimes (2010), ACS NANO **4**(3): 1259-1278.
- [7] Bell, T. Alexis, C. G. Bruce, R. Douglas and R. T. Michael (2008), No. PNNL-17214. Pacific Northwest National Laboratory (PNNL), Richland, WA (US).
- [8] Inoue, T., A. Fujishima, S. Konishi and K. Honda (1979), Nature **277**: 637-638.
- [9] Breault and Tanya M (2013). Diss. University of Michigan.
- [10] Wu, Z., Q. Wu, L. Du, C. Jiang and L. Piao (2013), Particuology.
- [11] A. K. Geim, Science, (2009), 324 (5934) 1530-1534.

- [12] J. I. Paredes, S. Villar-Rodil, A. Martínez-Alonso and J. M. D. Tascón, *Langmuir*, (2008), 24 (19), pp 10560–10564.
- [13] K. A. Mkhoyan, A. W. Contryman, J. Silcox, D. A. Stewart, G. Eda, C. Mattevi, S. Miller and M. Chhowalla (2009), *Nano Lett.*, 9 (3): 1058-1063
- [14] K. P. Loh, Q. Bao, G. Eda and M. Chhowalla, *Nat Chem*, (2010), 2 (12), 1015-24.
- [15] Tan, L. L., W. J. Ong, S. P. Chai and A. R. Mohamed (2013), *Nanoscale Research Letters* **8**: 465.
- [16] Štengl, V., S. Bakardjieva, T. M. Grygar, J. Bludská and M. Kormunda (2013), *Chemistry Central Journal* **7**(41).
- [17] Kazuya Nakata, A. F. (2012), *Journal of Photochemistry and Photobiology C: Photochemistry Reviews*.
- [18] Zhai, C., M. Zhu, F. Ren, Z. Yao, Y. Du and P. Yang (2013), *J Hazard Mater*: <http://dx.doi.org/10.1016/j.jhazmat.2013.1009.1013>.
- [19] Lewerenz, H. J., C. Heine, K. Skorupska, N. Szabo, T. Hannappel, T. Vo-Dinh, S. A. Campbell, H. W. Klemm and A. G. Munoz (2010), *Energy & Environmental Science* **3**(6): 748-760.
- [20] Inui and Tomoyuki (1996), *Catalysis today* **29**(1): 329-337.
- [21] Hummers Jr, William S and Richard E Offeman (1958), *Journal of the American Chemical Society* **80.6**: 1339-1339.
- [22] Huang, N., H. Lim, C. Chia, M. Yarmo and M. Muhamad (2011), *International Journal of Nanomedicine* **6**: 3443-3448.
- [23] Marcano, D. V. Kosynkin, J. M. Berlin, A. Sinitskii, Z. Sun, A. Slesarev, L. B. Alemany, W. Lu and J. M. Tour, *ACS NANO*, (2010), 4 (8), 4806-4814.
- [24] Liu, S., H. Sun, S. Liu and S. Wang (2012), *Chemical Engineering Journal*(214): 298-303.
- [25] S. Stankovich, D. A. Dikin, R. D. Piner, K. A. Kohlhaas, A. Kleinhammes, Y. Jia, Y. Wu, S. T. Nguyen and R. S. Ruoff, *Carbon*, (2007), 45 1558-1565.
- [26] Toyir, J.; Ramírez de la Piscina, P.; Fierro, J. L. G.; Homs, N. s. *Applied Catalysis B: Environmental* (2001), 34, 255-266.
- [27] Wolter, S. D.; Luther, B. P.; Waltemyer, D. L.; Önnéby, C.; Mohnéy, S. E.; Molnar, R. J. *Appl. Phys. Lett.* (1997), 70, 2156-2158.
- [28] Hee-Sung, K.; Reddy, M. S. P.; Dong-Seok, K.; Ki-Won, K.; Jong-Bong, H.; Yong Soo, L.; Hyun-Chul, C.; Jung-Hee, L., (2013), *J. Phys. D: Appl. Phys.*, 46, 155101.
- [29] Cho, S., J. Lee, I. Y. Park and S. Kim (2002), *Mater. Sci. Eng. B* **95**(3): 275-278.
- [30] Chen, X. and S. S. Mao (2007), *Chem. Rev.* **107**(7): 2891-2959.
- [31] Fabregat-Santiago, F., E. M. Barea, J. Bisquert, G. K. Mor, K. Shankar and C.A. Grimes
- [32] Leng, W. H., Z. Zhang, J. Q. Zhang and C. N. Cao (2005). *J. Phys. Chem. B* **109**: 15008-15023.
- [33] He, X. I., Y. Y. Cai, H. M. Zhang and C. H. Liang (2011). *J. Mater. Chem.* **21**: 475-480.
- [34] Benson, E. E., C. P. Kubiak, A. J. Sathrum and J. M. Smieja (2009), *Chem Soc Rev* **38**(1): 89-99.